Author responses to:

Interactive comment on revised "Modeling anaerobic soil organic carbon decomposition in Arctic polygon tundra: insights into soil geochemical influences on carbon mineralization" by Jianqiu Zheng et al.

Referee #1 (30 Oct 2018 report)

I would like to thank the authors for their rigorous work on addressing the comments on the early version. The manuscript is now significantly improved and easy to read. I have a minor editorial and two major considerations that will hopefully further enhance the quality of the manuscript.

We appreciate the reviewer's comments, which have improved this manuscript.

Major concerns:
- Authors have nicely responded to my comment on how hydrolysis process is implemented in the model. I understand that there is lack of data to implement hydrolysis step, independently. reason, authors have merged this step with fermentation process by assuming that hydrolysis is the rate limiting step, supported by observations from rice paddy soil. I was wondering how assumption could be for tundra and organic soil, the relevant systems, for this study. This assumption may contribute significant uncertainty for model predictions, since it regulates storage rate of Carbon. For instance, having microbial uptake as the rate limiting step may lead to substantial discharge and accumulation of oligomers depending on hydrological processes. Overall, carbon turnover rate and GHG emission rates over time.

As the reviewer notes, data are limited comparing rates of anaerobic hydrolysis versus substrate uptake in tundra soils. If microbial uptake were limiting during incubations, we would expect the accumulation of substrates in soil pore water. In our previous paper (Z. Yang et al. / Soil Biology & Biochemistry 95 (2016) 202) we measured a rapid decrease in reducing sugar and ethanol concentrations in pore water, correlated with the production of CO_2, CH_4 and organic acid fermentation products. When we added glucose to the depleted samples, gas production rates increased quickly. We interpret this result as a limitation in carbohydrate hydrolysis. We elaborated on this point in the revised manuscript on pages 3-4.

- The absolute values for many parameters are still not provided. I suggest presenting a table that includes all the parameters with values used or fitted from the simulation.

We added a new supplementary Table S1 "Model parameter values for reactions A1-A5." Also, the full model code is now available online:

Zheng, J., Thornton, P., Painter, S., Gu, B., Wullschleger, S., and Graham, D. E.: Modeling Anaerobic Soil Organic Carbon Decomposition in Arctic Polygon Tundra: Insights into Soil Geochemical Influences on Carbon Mineralization: Modeling Archive, Accessed at https://doi.org/10.5440/1430703, 2018.

This citation has been added to the manuscript.

- Minor: There are still numerous typo and grammar errors. I suggest a careful reading of the English.

We carefully proofread the revised manuscript, incorporating numerous small corrections –particularly in the references.

Referee #2 (6 Nov. 2018 report)
This study examines an integrated model simulating CO2 and CH4 production in permafrost soils and combines a first order linear decay model with a reaction kinetic simulation to look at effects of pH and fermentation on CO2 and CH4 flux. Overall this rewrite is easier to follow then the original version and model development easier to follow.

We thank the reviewer for productive comments, which we used to clarify and enhance this manuscript.

The authors still have not addressed how the model was tuned and I feel the model documentation could still be improved. This is, essentially, a model development paper since there is no hypothesis that is address with competing models or simulations scenarios. As such I would strongly suggest a table of equations summarizing the various pools which are tracked in the model associated parameters with how their ranges were derived. Relatedly there are vague statements about model fitting (page 5 line 40 specifically) but no actual algorithms given to reproduce parameterization.

We clarified that model optimization was performed using the least squares method by fitting with the observed CO2 production on p. 5, line 34. A description of various carbon pools that were adopted from a previous version of the CLM model with the decomposition cascade structure and parameters is described in Supplementary material (p.5). Furthermore, the complete model code with implementation instructions, input and output files is now available online for perusal (see DOI above).

Ideally I would also like to see a comparison with previous simpler models to motivate the added model complexity. The authors try to get around this with the correlation analysis but there demonstration of model improvement to give a sense of what the gap in the model-data fit was closed by this new formulation.

To characterize the improvements added to this model we introduced new simulations shown in supplemental Figure S10. Starting with a reference model that lacks new modules for iron reduction or dynamic pH calculation, we computed baseline values for CO_2, CH_4, TOAC and WEOC production, as well as pH and f_{pH} values. The added complexity of iron reduction interacted closely with dynamic pH calculations to produce simulations that better represented observed gas production and pH changes in the modeled incubations. These results shown in Figure S10 are briefly discussed in the main text (page 11, lines 30-38).

In the end the idea of combining a first order linear decay model with a reaction kinetic approach is intriguing and I'm left wanting more out of this paper.

Comparison of previous version (JuneRevised) with new version (DecRevised). Bibliography changes not shown due to full replacement.

Modeling anaerobic soil organic carbon decomposition in Arctic polygon tundra: insights into soil geochemical influences on carbon mineralization

Jianqiu Zheng[1], Peter E. Thornton[2,3], Scott L. Painter[2,3], Baohua Gu[2], Stan D. Wullschleger[2,3], David E. Graham[1,3]

[1]Biosciences Division, Oak Ridge National Laboratory, Oak Ridge TN, 37931 USA
[2]Environmental Sciences Division, Oak Ridge National Laboratory, Oak Ridge TN, 37931 USA
[3]Climate Change Science Institute, Oak Ridge National Laboratory, Oak Ridge TN, 37931 USA

Correspondence to: David E. Graham (grahamde@ornl.gov)

Abstract. Rapid warming of Arctic ecosystems exposes soil organic matter (SOM) to accelerated microbial decomposition, potentially leading to increased emissions of carbon dioxide (CO_2) and methane (CH_4) that have a positive feedback on global warming. Current estimates of the magnitude and form of carbon emissions from Earth system models include significant uncertainties, partially due to the oversimplified representation of geochemical constraints on microbial decomposition. Here we coupled modeling principles developed in different disciplines, including a thermodynamically based microbial growth model for methanogenesis and iron reduction, a pool-based model to represent upstream carbon transformations, and a humic ion-binding model for dynamic pH simulation to build a more versatile carbon decomposition model framework that can be applied to soils under varying redox conditions. This new model framework was parameterized and validated using synthesized anaerobic incubation data from permafrost affected soils along a gradient of fine-scale thermal and hydrological variabilities across Arctic polygonal tundra. The model accurately simulated anaerobic CO_2 production and its temperature sensitivity using data on labile carbon pools and fermentation rates as model constraints. CH_4 production is strongly influenced by water content, pH, methanogen biomass, and presence of competing electron acceptors, resulting in high variability in its temperature sensitivity. This work provides new insights into the interactions of SOM pools, temperature increase, soil geochemical feedbacks, and resulting CO_2 and CH_4 production. The proposed anaerobic carbon decomposition framework builds a mechanistic link between soil geochemistry and carbon mineralization, making it applicable over a wide range of soils under different environmental settings.

| Deleted: fermentations |
| Deleted: presented here |

1 Introduction

The northern permafrost region contains 1400-1800 Pg soil carbon (C), which is more than twice as much C as is currently contained in the atmosphere (Tarnocai et al., 2009; McGuire et al., 2012). Persistent cold and saturated soil conditions have limited

C decomposition in this reservoir. However, rapid warming and permafrost thaw exposes previously frozen organic carbon to accelerated microbial decomposition, potentially leading to emissions of carbon dioxide (CO_2) and methane (CH_4) that have a positive feedback on global warming (Zimov et al., 2006; Schuur et al., 2015; Schuur et al., 2009). How quickly frozen soil organic matter (SOM) will be mineralized, and how much permafrost C will be released to the atmosphere following thaw is highly

5   uncertain. Earth system models project 27 -508 Pg carbon release from the permafrost zone by 2100 under current climate forcing (Zhuang et al., 2006; Koven et al., 2015; MacDougall et al., 2012; Schaefer et al., 2014), varying by a factor of thirty. Understanding environmental dependencies of soil organic matter (SOM) decomposition is therefore essential for reducing model uncertainties and improving predictions of future climate change.

10   Disagreement in model projections for the northern permafrost region could be due to differences in model structure, model initialization, or parameters used in simulations. Despite increasingly detailed process representations in many models that simulate terrestrial CO_2 and CH_4 fluxes, important geochemical and metabolic constraints might still be poorly represented, oversimplified or missing in current biogeochemical models (Xu et al., 2016). The northern permafrost region is rapidly changing in response to the changing climate. Rising temperatures not only release more labile carbon from permafrost for decomposition, but also create

15   thermal and hydrological heterogeneity that further affects biogeochemical processes. Here we examine two mechanisms that substantially affect SOM turnover in permafrost-affected soils. First, rising temperature alters the kinetics of biogeochemical reactions (Segers, 1998). This effect is more pronounced at subzero temperature (Bore et al., 2017), and the process rate increase is higher at lower temperature ranges (Davidson and Janssens, 2006). Microbial communities also change with temperature, compounding effects on process rates (Karhu et al., 2014). Models address this temperature effect using empirical functions and

20   parameters (Tuomi et al., 2008; Xu et al., 2016), which might be highly biased depending on model assumptions and original curve fitting techniques, generating large uncertainties. Second, heterogeneity in permafrost thaw and related hydrological responses creates geochemical gradients in soils. Models use different levels of detail to simulate effects of water saturation (Meng et al., 2012; Xu et al., 2016). Soil moisture limits gas transport, and it is often used as an implicit control on heterotrophic respiration and methanogenesis. However, the explicit processes resulting from with soil oxygen depletion (e.g. soil redox status and pH dynamics)

25   are not widely represented (Riley et al., 2011; Meng et al., 2012; Xu et al., 2015).

The extent of SOM decomposition and gas emissions depends upon soil geochemical characteristics beyond temperature and O_2 availability. Among the wide range of environmental variables, pH emerges as a primary control on decomposition by regulating both microbial communities and microbial metabolic activities (Zhalnina et al., 2015; Jin and Kirk, 2018). pH affects microbial

30   metabolism by modulating the thermodynamics and kinetics of redox reactions. Redox reactions produce or consume protons, and thus, their free energy yields vary with pH (Bethke et al., 2011; Jin and Bethke, 2007). The Gibbs free energy available to anaerobic microorganisms that degrade simple organic molecules generally increases (becomes less favorable) with increasing pH (Bethke et al., 2011). Notably, iron [Fe(III)] reduction is highly proton consuming and becomes less favorable at higher pH (Figure S1). Previous studies identified iron reduction as a major process in anoxic Arctic soils (Lipson et al., 2010; Lipson et al., 2013), which

35   increases local pH and might favor co-occurring methanogenesis (Tang et al., 2016; Wagner et al., 2017). However, the influence of iron reduction on methanogenesis rates in different soils is rarely investigated. The reactivity of iron and its pH-feedback impose additional complexity on the controls of SOM decomposition and associated CH_4 production.

Despite the importance of pH in controlling redox reactions and resulting C emissions, pH change is not explicitly represented in

40   biogeochemical models. Most of the current biogeochemical models apply a single initial pH value for redox reactions without considering proton production and consumption during the processes. Traditional decomposition models use landscape position, soil moisture content, or other proxies for O_2 concentration to determine the form of C release. Scalars on aerobic respiration (Riley

4

et al., 2011; Lawrence et al., 2015) or empirical ratios of CO_2 and CH_4 (Koven et al., 2015) are often used to inform the extent of C decomposition and partitioning of CO_2 and CH_4 production. Reactions that produce or consume protons and the resulting pH changes or ion exchange reactions are not considered in these empirical models. Some process-rich models explicitly include details of methanogen populations and their interactions with substrates and other environmental factors, but these models still lack the capability to simulate pH changes during long-term carbon decomposition. Instead, constant pH is often assumed within bell-shaped pH response functions (Meng et al., 2012; Tian et al., 2010; Xu et al., 2015). Without underlying proton exchange and pH buffering mechanisms, a significant error may occur when rate calculations depend heavily upon the initial choice of a single optimal pH value for various reactions.

In this study we developed a new anaerobic carbon decomposition model framework with explicit representation of aqueous phase geochemistry to allow pH and thermodynamic calculations. By coupling three different models, including a thermodynamically based microbial growth model, a substrate pool-based model, and a humic ion-binding model, we built a process-rich carbon decomposition model that allows simultaneous thermodynamic and pH calculations. Results from anoxic incubations of permafrost affected soils along a hydrological gradient were synthesized to parameterize and validate this new model framework. The main objectives of this study were to (i) examine the role of soil geochemical variables in controlling anaerobic carbon decomposition and carbon release (as both CO_2 and CH_4); (ii) develop a common set of parameters in the new anaerobic carbon decomposition framework to capture variabilities in CO_2 and CH_4 production; and (iii) evaluate model uncertainties in responses to both soil heterogeneity and model parameterization, emphasizing effects of soil saturation, pH and temperature response.

2 Materials and methods

2.1 Anaerobic carbon decomposition model

The anaerobic carbon decomposition framework was developed with explicit representation of fermentation, methanogenesis and iron reduction, which were identified as key mechanisms for anaerobic CO_2 and CH_4 production . The main structure of this framework included two major components: a simplified CLM-CN decomposition cascade (Converging Trophic Cascade, or CTC) (Thornton and Rosenbloom, 2005) to facilitate parameterization of the upstream carbon flow entering the aqueous phase dissolved organic carbon (DOC) pool (Figure 1, process 1), and an aqueous phase to facilitate calculations of thermodynamics and redox-reaction associated acid-base chemistry. An empirical approach was used to represent non-aqueous phase SOC decomposition. Additionally, mechanistic representations of methanogenesis and iron reduction were developed in this work based on aqueous phase thermodynamic calculations.

The simplified CTC cascade included 4 SOM pools to represent bulk SOC with different levels of complexity. Changes of these SOM pools followed modified first-order-decay (see Supplementary Material for details). We modified the original respiration fraction (Thornton and Rosenbloom, 2005; Koven et al., 2013) into direct and indirect fractions. Thus for each SOM pool, the direct respiration fraction represented CO_2 lost as orgnially defined, while the indirect respiration fraction was labile C produced from bulk C entering the aqueous phase carbon pool (DOC pool, Figure 1).

The large biomolecules in the DOC pool went through multiple hydrolysis and fermentation steps to produce low molecular weight organic acids that would further respire into CO_2 and CH_4 (Boye et al., 2017; Zheng and Graham, 2017; Roy Chowdhury et al., 2015; Yang et al., 2016). Under anoxic conditions, hydrolysis of polysaccharides was considered the rate-limiting step for downstream methanogenesis (Glissmann and Conrad, 2002). Polysaccharide hydrolysis has a favorable free energy, due to

5

increased entropy, but cannot be readily coupled to biological energy transduction outside of the cell. We previously measured a rapid decrease in reducing sugar concentrations in pore water during tundra soil incubations, which indicated that hydrolysis limits decomposition . At low temperature (below 15 °C), the microbial degradation of cellulose was considerably diminished while other polymers, such as starch or proteins, were degraded much faster at low temperature, resulting in the accumulation of organic acids,

5   primarily acetic, propionic and butyric acids (Kotsyurbenko, 2005;Yang et al., 2016). These low molecular weight organic acids further fueled microbial mineralization reactions that led to production of CH_4 and CO_2. Given that most anaerobic lignocellulose degraders also fermented sugars following hydrolysis (Blumer-Schuette et al., 2014), we assumed the turnover of DOC into low molecular weight organic acids was a single lumped fermentation process (Figure 1, process 2), in which labile DOC ($C_6H_{12}O_6$) was fermented into acetate, H_2 and CO_2 (Appendix A, reaction A1 and Table S1). This assumption gave a fixed stoichiometry

10   ratio, 1/3 of the fermented carbon was oxidized to CO_2.

Redox reactions including methanogenesis and iron reduction were represented using a thermodynamically-based approach (Istok et al., 2010), with unique microbial growth kinetics incorporated into energy yielding redox reactions. In this thermodynamically based approach, the growth equations of methanogens and iron reducers were derived from paired electron donor (acetate or H_2)

15   and electron acceptor half reactions and a biomass synthesis equation (Istok et al., 2010). Using a constant molecular formula as biomass ($C_5H_7O_2N$), and ammonium (NH_4^+) as the nitrogen source for biosynthesis, we derived the growth equations for methanogenesis and iron reduction (Appendix A, equation A2-A5). Rate calculations followed the generalized Monod rate law (Jin and Bethke, 2007) with an additional thermodynamic factor representing the thermodynamic driving force. The thermodynamic factor $f(G)$ is calculated using equation 1 (Jin and Bethke, 2003):

20

$$f(G) = 1 - \exp\left(-\frac{-\Delta G - m\Delta G_p}{\chi RT}\right) \tag{1}$$

where ΔG [kJ (mol reaction)$^{-1}$] is the free energy change of the redox reaction. ΔG depends on the standard Gibbs free energy change (ΔG^0) and the concentrations of chemical species involved in the reaction. ΔG_p is the phosphorylation potential, i.e., the energy required to synthesize ATP to ADP and dihydrogen phosphate in cell's cytoplasm. ΔG_p is about 45 kJ (mol ATP)$^{-1}$ (Jin

25   and Kirk, 2018). m is the number of ATP molecules synthesized per redox reaction. χ is the average stoichiometric number (Jin and Kirk, 2018), R is the gas constant (kJ mol^{-1} K^{-1}), and T is the absolute temperate (K). This factor $f(G)$ ranges from 0 to 1, where the reaction is thermodynamically favorable when $f(G) > 0$.

Both methanogenesis and iron reduction contribute to pH change. Reactions such as ferrihydrite reduction substantially increase

30   alkalinity (Appendix A, Reaction A4, A6). Furthermore, the solubility of CO_2 and the composition of dissolved CO_2 and bicarbonate vary significantly over typical soil pH values, affecting all C mineralization processes. In the organic-rich soils modeled here, SOM rather than minerals provides most buffering capacity. Therefore, we used the humic ion-binding model to describe pH buffering during carbon decomposition. A simplified parameterization of proton binding is available in the Windermere Humic Aqueous Model (WHAM,), which has been extensively calibrated to represent the acid-base chemistry of

35   "average" humic and fulvic acids, and benchmarked with heterogeneous natural organic matter (Atalay et al., 2009). We adopted the WHAM parameterization to represent proton binding characteristics (pH buffering) provided by SOM (Tang et al., 2016). Using representative binding constants provided by WHAM, the pH buffering capacity can be directly adjusted by altering the number of proton binding sites, which is assumed to be linearly correlated with the total amount of SOM (see Supplementary Material for details).

40

2.2 Model implementation and initialization

Deleted: lead

Deleted: that

Deleted: respired as

Deleted: and

Deleted: [Δ

Deleted:),

Deleted:], and

Deleted: ATPs

Deleted: Tipping, 1994; Tipping, 1998),

The above model structure was implemented using the open source geochemical program PHREEQC 3.0, with a new database describing SOC decomposition cascade, redox reaction kinetics and pH buffering (*redox.dat*, available at https://github.com/jianqiuz/decomposition). This model assumed thermodynamic equilibrium of aqueous chemical speciation, mineral dissolution/precipitation, and ion sorption/desorption based on the updated PHREEQC thermodynamic database (*phreeqc.dat*,). The database was modified to include WHAM pH buffering and reaction kinetics for SOM pools decay and reaction kinetics for fermentation, methanogenesis and iron reduction. The kinetic rate constants and microbial biomass growth and decay rates were adopted from former thermodynamically based studies (Istok et al., 2010) and previously tested with low-center polygon Arctic soils (Tang et al., 2016).

The model initialization was based on both the incubation conditions and soil geochemical characterizations (Figure S2). The initial partitioning of SOM pools was assumed to be at fixed ratios due to the limitation of short-term incubation data. Under the experimental conditions, we assumed SOM1 and SOM2 pools with relatively shorter turnover rates (τ =14 days and 70 days, respectively) were most relevant in the model. On the other hand, SOM3 and SOM4 pools were relatively inert ($\tau > 2$ years for both pools). We started with the relative fractions of SOM pools at approximately 10%, 40%, 10% and 40% of SOC in organic and mineral soils for SOM1-4. We further assessed the bias of this assumption with sensitivity analysis. Sizes of SOM1 and SOM2 pools were reduced by 90% for permafrost to better account for the overall low levels of carbon degradation.

All other variables required were initialized using measurements based upon 10 to 15 g of wet soil incubated in 60 to 70-mL sealed bottles. Total soil organic carbon (SOC), total water (TOTW), total organic acid carbon (TOAC), pH and the initial concentration of Fe(II) were specified in the model based on measurements (Table S2). The DOC pool in the model was initialized using the measured water extractable organic carbon (WEOC) expressed as a fraction of SOC (f_{doc}). On average, WEOC accounts for approximately 2% of SOC based on our synthesized data (see section 3.1). This value is consistent with previous long-term incubations, which suggested less than 5% of SOC was fast decomposing carbon in permafrost affected soils at a standardized temperature of 4-5 °C (Knoblauch et al., 2013; Schädel et al., 2014). The starting biomass of methanogens and iron reducers was assumed to be within the range of 10^{-3} to 10^{-5} gC/gSOC for organic soils, 10^{-4} to 10^{-6} gC/gSOC for mineral soils, and 10^{-7} to 10^{-9} gC/gSOC for permafrost (Table S2). This stratified microbial biomass distribution was used to represent the vertical gradient in the relative abundance of microbial communities (Treat et al., 2014; Waldrop et al., 2010; Yang et al., 2017).

The lumped fermentation process was the rate-limiting step in the model and was fitted individually with data from each soil microcosm. Based upon reaction stoichiometry, the fermentative conversion of each mole of labile C led to 2/3 mole of organic acids and 1/3 mole of CO_2. Organic acids were mineralized via methanogenesis or iron reduction to convert approximately 49% to 88% of C in organic acids into CO_2. This estimation was based on reaction stoichiometry of A2 and A4, and a fraction of the C was incorporated into microbial biomass. Therefore, the percentage of respired C would be less than 100% even if all organic acids were respired as CO_2. If we assume all fermentation products were mineralized into CH_4 and CO_2, we could estimate the fermentation rate (R_{fer}) from measured CO_2 production. Thus, R_{fer} was estimated using the initial CO_2 production rate in the incubation data, and further optimized using the least squares method by fitting with observed CO_2 production values (Table S3).

Temperature and pH response functions were used to further constrain model simulations (Figure S2). A temperature effect was parameterized using the CLM-CN temperature response function (Appendix B, equation B1). Additional temperature response functions were evaluated by sensitivity analysis (see section 2.4). The effect of pH on biological reaction rates is modulated by bell-shaped pH response functions (Tang et al., 2016; Xu et al., 2016). Here we used the Dynamic Land Ecosystem Model (DLEM)

7

pH response function (Appendix B, equation B5), since it generated the least variation in parameter perturbation tests (Tang et al., 2016).

2.3 Incubation data synthesis for model validation

5   Incubation data from Utqiaġvik (Barrow) Alaska soil cores that represent the microtopographic heterogeneity of polygona tundra were synthesized to validate the new anaerobic carbon decomposition model. The selected datasets represent fine scale variabilities in thermal and hydrological regimes across the gradient of soil microtopographic positions (Herndon et al., 2015). The synthesized data contains complete sets of soil geochemical descriptions for organic, mineral, transition zone (if identified) and permafrost layers from each microtopographic feature (see Supplementary Material for details). Levels of total soil organic carbon, WEOC,

10 and TOAC were available before and after soil incubation. Besides CH_4 and CO_2 production during low temperature soil decomposition, data on Fe(II) concentrations and pH changes were also available for model initialization and validation.

2.4 Model parameter uncertainty

This model was designed as a generic framework to simulate anaerobic carbon decomposition across a range of soil physiochemical conditions. Two types of sensitivity analysis were conducted to evaluate model performance. First, possible bias and variations

15 associated with model initialization variables (soil geochemical attributes) were assessed using perturbation simulations. Variations of ±25% and ±50% (+100% and 200% for some variables) were applied to these variables, and the resulting changes in cumulative CO_2 and CH_4 production were evaluated by comparing with reference simulations. This evaluation helps to identify critical measurements needed for initializing the model. Second, parameters specifically benchmarked in this study and parameters adopted from empirical relationships were also evaluated with perturbation simulations. This test helps to apportion the model prediction

20 uncertainties into different sources, including model input, parameters, or model structure.

3 Results

3.1 Meta-analysis to validate model assumptions

Incubation data used in this study were generated from soils representing different microtopographic features with a wide range of moisture and SOC contents and reported elsewhere. Correlation analysis revealed a close relationship between soil moisture and

25 organic carbon pools (measured as SOC, WEOC and TOAC) among examined soil microtopographic features and across soil depth (p < 0.01, Table S4). All these soil properties significantly correlated with cumulative CO_2 and CH_4 production (p <0.05), suggesting the important role of initial soil geochemical properties in controlling carbon degradation.

Although various levels of carbon mineralization were measured as CO_2 and CH_4 production during incubations, changes in WEOC

30 and TOAC were consistent among treatments with distinct patterns. WEOC represents 0.3% to 2.6% of total SOC among all test soils, and this ratio remained constant before and after anoxic incubations (Figure S3). On the other hand, TOAC showed much more dynamic changes among different soils and different incubation temperatures. TOAC generally increased in soils from organic layer, transition zone and permafrost. In contrast, TOAC drastically decreased by up to 90% in mineral soils. These results indicate that WEOC was in a steady state among examined soils, while TOAC varied substantially due to microbial mineralization

35 processes, supporting the model assumption of lumped fermentation (the conversion of WEOC to TOAC) as the rate limiting step.

Deleted: generates

Deleted: water extractable organic carbon (

Deleted:)

Deleted: total organic acid carbon (

Deleted:)

Deleted: is

Deleted: (Roy Chowdhury et al., 2015; Zheng et al., 2018).

Deleted: S2

Deleted: showed significant correlation

Deleted: assumptions

Both CO_2 and CH_4 production rates responded strongly to rising incubation temperature (p =0.02 and p =0.04, respectively, Figure S4, Tables S5 and S6). The estimated Q_{10} values of CO_2 production showed a relatively narrow range while methanogenesis had much larger variation in estimated Q_{10} values ranging from 1.6 to 48.1. Using Q_{10} values to simulate the temperature dependence of processes might work for CO_2 production, but could generate significant errors in predicting CH_4 production.

3.2 Modeled CO_2 and CH_4 production using observed parameters

The model performed well in simulating CO_2 and CH_4 dynamics across a range of moisture and SOC gradients and among different soil types (Figures S5 and S6). Variations in gas production among different conditions, including microtopographic features, soil layers, and different incubation temperatures were well captured (Figure S7). The comparisons between modeled and observed CO_2 and CH_4 production are shown in Figure 2. The model slightly underestimates CO_2 production towards the end of the incubations, but still maintains a good agreement between modeled and observed CO_2 production (R^2=0.89). The underestimation of CO_2 production is likely due to substrate limitations caused by the initial distribution of different carbon pools. Model-predicted CH_4 production also showed good agreement with observations (R^2=0.79). More variation between modeled and observed CH_4 production suggests a systematic pattern in the model parameterization of methanogenesis: the model underestimates CH_4 production at 4 and 8 °C, and overestimates CH_4 production at -2 °C.

To assess the model sensitivity to initial model inputs, we compared model predictions in response to varying initial model inputs via perturbation simulations. First, we examined the influence of the partitioning of different carbon pools. Significant changes in model predictions of CO_2 and CH_4 were observed in response to perturbations of initial input of SOC, WEOC, but not TOAC (Figure 3). SOC determines the size of different carbon pools in the model, and it further influences the predictions of WEOC, TOAC, CO_2 and CH_4. For example, predicted CO_2 and CH_4 production increased by about 200% when +200% changes were applied to initial SOC input. This trend is consistent with correlation analysis of incubation results, described above (Table S4). Perturbations in initial WEOC strongly altered the predictions of TOAC and CO_2, consistent with the model assumption of the conversion of WEOC to TOAC (fermentation process) as the rate-limiting step. The model also predicted increases in CH_4 and Fe(II) accumulation in response to lower WEOC. Lower WEOC significantly reduced organic acid accumulation, and thus increased system pH and accelerated rates of both methanogenesis and iron reduction. The starting level of TOAC showed minimal influence on model predictions of CO_2 and CH_4, suggesting other factors rather than substrate availability were limiting carbon mineralization. The initial sizes of SOM1 and SOM2 pools showed very slight changes in model predictions of WEOC and CO_2, and minimal influence on CH_4 prediction, further supporting the assumption that downstream fermentation is the rate-limiting step in the model. Additional soil geochemical factors, including soil moisture, Fe(II) and pH also significantly influence model output. In particular, initial soil pH showed a dramatic effect on predicted CO_2 and CH_4 production. With initial soil pH increased from 5 (reference simulation) to 6, the model predicted 160% and 308% increase in CO_2 and CH_4 production, respectively. Perturbations in initial soil pH had the strongest effect on the prediction of CH_4 by assigning different values in f_{pH} that were directly proportional to the methanogenesis rates. The above results of perturbation simulations demonstrated high sensitivity of this model in response to varying soil geochemical properties.

3.3 Model sensitivity to parameterization uncertainties

To further validate the model, we performed additional sensitivity analysis to justify model assumptions and estimate the uncertainties generated from model parameterizations. One major assumption of this modeling framework is to lump multiple fermentation processes into one reaction stoichiometry, controlled by one reaction rate constant. It is critical to evaluate how this

simplified structure influences model performance and contributes to model output uncertainties. The model parameter sensitivity analysis indicated the TOAC pool was most sensitive to changes in the fermentation rate (R_{fer}) and reaction stoichiometry (Figure 4). Downstream reactions were less affected by the uncertainties of the two tested parameters. These results supported our assumption of lumped fermentation with fixed stoichiometry, indicating the robustness of the model structure presented here.

5

The selection of temperature response functions represents one of the major sources of model uncertainties. A sensitivity analysis was performed by comparing four different temperature response functions (Appendix B). In our simulations, the quadratic temperature response function proposed by Ratkowsky et al. predicted much higher CO_2 and CH_4 production rates at higher temperature, and the lowest rates of both CO_2 and CH_4 at temperatures below 0 °C, giving the highest temperature response among

10 tested response functions (Figure 5). In contrast, the Arrhenius equation predicted much lower temperature response for both CO_2 and CH_4. Empirical functions used in CLM-CN and CENTURY models gave similar temperature responses for both CO_2 and CH_4. Variations in low temperature CO_2 production are well constrained by established temperature response functions, while CH_4 production at -2 °C showed a much wider range of temperature response, and the median value is best simulated using the Ratkowsky function. This sensitivity analysis is consistent with model output of CO_2 and CH_4 production, where CO_2 is well

15 constrained by the model, but CH_4 is significantly overestimated at -2 °C using the CLM-CN temperature response function. A unified temperature response function for all reactions under different biotic or abiotic constraints substantially contributes to the disagreement between model output and observations.

Redox reactions contribute to proton production or consumption, and the resulting pH alters the value of the pH response function

20 (f_{pH}) that directly controls reaction kinetic functions, creating a feedback loop. pH buffering capacity (BC) provided by SOM with proton binding sites and f_{pH} represent two major sources of uncertainties in this feedback loop. Thus, we performed perturbation simulations to characterize the sensitivity of model output to variations in BC and f_{pH} (Figure 6). Higher BC stabilized system pH during prolonged incubations, while lower BC permitted a pH increase by up to 0.71 pH unit compared to the reference simulation. This 14% pH increase led to a 123% increase in f_{pH}, accelerating both methanogenesis and Fe(III) reduction rates substantially.

25 Perturbations on the pH response function were directly reflected in the slopes of pH response curves (Figure S8). We found up to 372% change in the value of f_{pH} during a 60-day simulation, as a steeper increase in f_{pH} accelerated both methanogenesis and iron reduction (equation A2-A5), which contributed to pH rise that further accelerated f_{pH} increase. Correspondingly, both CH_4 and Fe(II) increased by more than 100% after the simulation. While BC is an important factor controlling both redox reactions and pH fluctuations, a unified f_{pH} for all reactions may impose significant variations in model output.

30

BC is an intrinsic soil property simulated with a simplified linear relationship to soil SOM. However, it generates a strong nonlinear response in the simulations of methanogenesis and Fe(III) reduction (Figure 7a). Simulations with varying soil BC revealed dynamic pH change at lower BC (Figures 8 and 9, with BC=1 as reference simulation, and stabilized pH at higher BC. At constant temperature, rates of both methanogenesis and Fe(III) reduction increased significantly at lower BC due to pH control. At lower

35 BC when pH change is not well buffered, higher pH accelerated CH_4 and Fe(II) production rates (Figure 7), giving much higher apparent temperature responses, while at higher BC with stabilized pH in the system, apparent temperature responses of these redox processes were significantly lower than the reference simulation (BC=1). Variations in pH buffering capacity generated large variations in apparent temperature responses of methanogenesis and Fe(III) reduction due to this pH feedback loop.

4 Discussion

40 **4.1 Synthesized soil geochemistry and model validation**

10

Deleted: rate

Deleted: response

Deleted: is

Deleted: in the loop,

Deleted: accelerating

Deleted:),

Deleted: the

Soil geochemical characteristics represent important abiotic controls on anaerobic carbon decomposition and subsequent CO_2 and CH_4 production. SOC content, soil pH, water table position, C:N ratio, and landscape position were all suggested to contribute to the variability in anaerobic CO_2 and CH_4 production (Lee et al., 2012; Schädel et al., 2014; Treat et al., 2015). We synthesized incubation data for gelisol soils from different pedons and soil moisture regimes representing heterogeneity across the Barrow

5 Environmental Observatory (BEO). This coordinated data set allowed us to focus on individual factors and their roles in relation to anaerobic CO_2 and CH_4 production.

Carbon released as CO_2 and CH_4 during anoxic incubations decreased with depth. Permafrost was associated with low levels of CO_2 production and very low CH_4 production, consistent with a previous synthesis (Treat et al., 2015). Nevertheless, permafrost

10 TOAC, WEOC, and SOC concentrations were all comparable to organic soils, suggesting high substrate availability but low microbial activity. This trend is consistent with previous studies, where highest microbial abundance and diversity were observed in surface soil, and permafrost contained low microbial abundance (Treat et al., 2014; Waldrop et al., 2010). Among surface soils, higher moisture in low-centered polygon soils significantly promoted CO_2 and CH_4 production and the accumulation of fermentation products (measured as TOAC), emphasizing the importance of soil SOC content and moisture as strong

15 environmental drivers for carbon decomposition. Given the bias in correlation analysis created by the skewed distribution of CO_2 and CH_4 production in our dataset, additional cluster analysis was performed based on data similarity rather than correlations. High similarity of soil attributes (depth, moisture, pH, C:N ratio, SOC, TOAC) with CH_4 production (Figure 8a) was found, suggesting methanogenesis is potentially controlled by a set of soil geochemical characteristics in the local microenvironment.

20 These synthesized observations support the major assumptions of our model development: (1) the coupled hydrolysis and fermentation processes converting macromolecular SOM into low molecular weight organic acids is the rate limiting step; and (2) different rates of CO_2 and CH_4 production from different soil layers can be attributed to variations in microbial activity manifested as differences in initial microbial biomass or growth rates. Additional observations of substantial Fe(III) reduction and associated pH increases during anaerobic decomposition (Figure S9) confirmed the need to simulate pH variations associated with redox

25 reactions and corresponding microbial responses. This anaerobic carbon decomposition framework adequately modulated the involved biotic and abiotic interactions by splitting the carbon flow to different redox reactions and simulating pH buffering capacity to mediate associated changes in acidity or alkalinity.

The model presented here identified fermentation, acetoclastic methanogenesis and acetotrophic iron reduction as key mechanisms

30 for anaerobic CO_2 and CH_4 production (Vaughn et al., 2016; Lipson et al., 2010). Although denitrification, ammonification and sulfate reduction are all thermodynamically more favorable, low nitrate and sulfate concentrations in BEO soils limit flux through these pathways (Newman et al., 2015). We performed another cluster analysis on the model output (Figure 8b), where we not only simulated fermentation, methanogenesis and iron reduction rates and associated pH changes, but also tracked the biomass of methanogens (M_Meb) and iron reducers (M_Feb). A dendrogram depicting data similarity showed four distinct clusters consisting

35 of WEOC, CO_2 (CO_2 prediction), Ferrous (Fe(II) prediction), and CH_4 (CH_4 prediction) that closely associated with soil geochemical properties and incubation temperature. This result is similar to the cluster analysis of synthesized data, demonstrating that the proposed model structure captured major relationships between carbon mineralization and soil geochemical attributes. Predicted CH_4 production is strongly influenced by incubation temperature, soil pH, soil moisture, and depth that determine the size of the methanogen population. This model prediction is consistent with previous studies on the vertical distribution of

40 methanogen population (Waldrop et al., 2010). Environmental factors, such as labile organic matter, water table depth, and soil redox status, soil alkalinity and salinity (Wachinger et al., 2000; Rivkina et al., 2007; Høj et al., 2006; Yang et al., 2017) are all likely to contribute to the variabilities in the distribution and abundance of methanogens and subsequent methane production.

11

Deleted: .

Deleted: (Walz et al., 2017; Treat et al., 2015),

Deleted: acetotrophic

Deleted: comprising

Deleted: further validating

Deleted: in capturing

Deleted: and

Deleted: determines

4.2 Temperature and pH response of anaerobic carbon decomposition

Rising temperature promotes anaerobic carbon decomposition, resulting in increased rates of anaerobic CO_2 and CH_4 production (Treat et al., 2014; Lupascu et al., 2012). It is widely recognized that methanogenesis is more sensitive to temperature than respiration (Yvon-Durocher et al., 2014; Yvon-Durocher et al., 2012), and it is usually associated with large variations. Segers
5 estimated the Q_{10} value of methanogenesis ranged from 1.5 to 28 among 1043 incubation experiments using wetland soils (Segers, 1998). Our data synthesis revealed higher temperature sensitivity than other reported values. High estimated temperature sensitivity across the freezing point of water has previously been documented (Waldrop et al., 2010) and further attributed to limited water availability for microbial activities at sub-zero temperature (Tilston et al., 2010). Ratkowsky et al. proposed a quadratic relationship for the temperature dependence of microbial growth rates that modeled low-temperature growth better than the Arrhenius Law
10 (Ratkowsky et al., 1982). Our simulations suggest better prediction of methanogenesis with this temperature response function, possibly due to a more suitable representation of growth limitation of methanogens at sub-zero temperature. Methanogenesis rates are also influenced by the availability of alternative electron acceptors and carbon source. Processes contributing to the accumulation or consumption of carbon substrates and competing electron acceptors may respond differently to temperature change, which could further complicate the temperature sensitivity of methanogenesis. Current modeling approaches heavily
15 depend upon empirical temperature response functions, which may be associated with large uncertainties due to variations in the selection of data and curve fitting methods. Extrapolation of carbon decomposition rates, particularly methanogenesis rates, into a future warmer climate remains uncertain. More accurate simulations will require additional information on geochemical properties that contribute to the variations of methanogens distribution and methanogenesis activity.

20 pH values impose fundamental physiological restrictions on microbial activities. Soil pH ranges from acidic to circumneutral (pH 4-7.5) in northern Alaska and varies substantially through the soil profile and along the microtopographic gradient. Accumulation of organic acids in anoxic soils leads to pH decline (Jones et al., 2003), while consumption of organic acids by methanogenesis and iron reduction increases the alkalinity of the system via the production of HCO_3^- and OH^- (Drake et al., 2015; Roy Chowdhury et al., 2015; Howell et al.). The interplay of these processes leads to strong nonlinear pH feedbacks in the system, and previous
25 studies have observed up to 1-2 pH unit changes during short-term anoxic incubations (Xu et al., 2015; Drake et al., 2015; Roy Chowdhury et al., 2015). These relationships between pH and organic carbon decomposition can vary in sign and magnitude. Our model simulations with mechanistic pH evolution indicate that constant pH assumed in previous models may cause significant errors in simulating long-term anaerobic CO_2 and CH_4 production. The intrinsic soil pH buffering capacity plays a large role in stabilizing soil pH and may vary depending upon solution acidity or alkalinity, cation exchange capacity, SOM content and mineral
30 composition and/or dissolution. These properties derive from SOM characteristics, moisture, mineral content, and additional geochemical properties, leading to complex correlations between soil pH and SOC decomposition rate that require future investigation.

4.3 Fast-decomposing carbon pool
35

Substrate availability is a primary determinant of potential CO_2 and CH_4 production (Lee et al., 2012; Schuur et al., 2015; Tarnocai et al., 2009). Total SOC is composed of heterogeneous C pools characterized by different turnover times. Carbon release during short term incubation originates from the C pool with relatively rapid turnover. The size and turnover time of this quickly-metabolized carbon pool is usually estimated by two-pool or three-pool conceptual models with a maximum likelihood solution
40 using time series of CO_2 data (Schädel et al., 2013). A previous study on Siberian permafrost soils using a two-pool model estimated a turnover time of 0.26 years for the fastest-responding pool (Knoblauch et al., 2013). A three-pool model was applied using more

12

Deleted: even

Deleted: be heterogeneous

Deleted: residual acidity or

extensive incubation datasets collected from 23 high-latitude ecosystems, yielding an estimate of 0.35 years mean turnover time for the fastest-responding carbon pool (Schädel et al., 2014).

In our synthesis study, we directly quantified WEOC and assumed it represented the fast-decomposing labile carbon pool. The size of the labile carbon pool is constant during anaerobic decomposition, while total CO_2 and CH_4 release represent up to 194% of the labile carbon pool, indicating continuous replenishment of labile carbon pool from non-labile carbon pools within the hierarchy. The replenishment of labile carbon pool can be attributed mostly to decomposition of SOM1 and SOM2 pools with faster turnover (Koven et al., 2013). Overall, we estimated the fast-decomposed carbon pool is approximately 2-4% of total SOC, similar to previous estimates. The turnover time calculated from the fermentation rate was comparable to estimates of the turnover time of the fastest-responding carbon pool in previous studies (Figure 9), suggesting these quantifications and parameterization in the anaerobic carbon decomposition framework apply broadly.

4.4 Key features of the anaerobic model framework and future considerations

Here we present an anaerobic carbon decomposition framework by combining three well-known modeling approaches developed in different disciplines. A pool-based model to represent upstream carbon transformations and replenishment of a DOC pool, a thermodynamically-based model to calculate rate kinetics and biomass growth for methanogenesis and Fe(III) reduction, and a humic ion-binding model for aqueous phase speciation and pH calculation are implemented into the open source geochemical model PHREEQC. The model framework presented here has several unique features. First, this model is built upon a thermodynamically-based approach, which allows consistent parameterization of individual reactions along the redox ladder. Such a model structure is particularly useful in circumstances when function-specific microbial growth is difficult to quantify and parameterize. Second, calculations of free energy changes of redox couples are used to modulate redox reaction hierarchy. Considering the difficulty in obtaining growth-associated parameters for every functional group, a thermodynamically-based approach significantly decreases the number of parameters that are difficult to measure. In addition, proton production and consumption during redox reactions are incorporated into a dynamic pH calculation, allowing various simulations on aqueous solubility and reactivity of different elements. The anaerobic carbon decomposition framework presented here holds a significant advantage over traditional models in simulating carbon decomposition process within a wide range of environmental settings.

In permafrost affected regions, studies consistently identify iron reduction, denitrification and sulfate reduction (Lipson et al., 2010; Lipson et al., 2013; Ernakovich et al., 2017; Hansen et al., 2007) as alternative anaerobic pathways, which are recognized as energetically more favorable processes than methanogenesis. Fe reduction makes a significant contribution to total respiration (Roy Chowdhury et al., 2015; Herndon et al., 2015), and adding Fe reduction simulations to a baseline model (without Fe reduction or dynamic pH calculations) caused faster decreases in TOAC and WEOC pools and increased CO_2 production as expected (Figure S10). More indirect feedbacks were revealed when dynamic pH calculation was enabled. With dynamic pH simulation during anaerobic decomposition, the model revealed strong pH dynamics that are counterbalanced by Fe reduction. By including both Fe reduction and dynamic pH calculations, the model accurately reproduced the initial pH drop and subsequent pH rise during incubations, which were commonly observed in permafrost affected soils (Roy Chowdhury et al., 2015; Herndon et al., 2015). The new model framework presented here provides a basis for a deeper understanding of carbon decomposition under oxygen-limited conditions where the importance of accounting for alternative election acceptors and pH feedbacks becomes more pronounced. Future fine-scale experiments on carbon decomposition using alternative electron acceptors would be beneficial for more comprehensive parameterization of this model framework. Additional observations on temperature and pH sensitivity of specific redox reactions would also be quite useful in reducing large uncertainties generated by the current representation of temperature and pH responses. Application of such a modeling framework at the field scale requires close coupling with hydrology models to

13

facilitate estimations of aqueous phase concentrations. Additional assumptions on vertical mixing and gas diffusion in the soil column should also be considered.

5. Conclusion

5   Microbial processes are the driving forces for biogeochemical cycling of soil carbon and are subjected to environmental constraints beyond temperature and organic substrate availability. The present study incorporated microbial redox reactions and mechanistic pH evolution to simulate anaerobic carbon decomposition in Arctic soils with depth and across soil moisture gradients. Our data synthesis and modeling results quantify direct effects of temperature on anaerobic carbon decomposition, as well as indirect effects of soil geochemistry that cause strong redox reaction-pH feedback. We identified substantial pH feedbacks on the predictions on

10 CO_2 and CH_4 production. The anaerobic carbon decomposition framework presented in this study provided the essential model structure to incorporate redox reactions of alternative electron acceptors for accurate simulation of CO_2 and CH_4 production. Soil geochemistry imposes critical constraints on SOM decomposition, and further regulates permafrost carbon feedback in response to changing climate.

Code and data availability

15 PHREEQC (Version 3) is publicly available at http://wwwbrr.cr.usgs.gov/projects/GWC_coupled/phreeqc/

The model is archived at https://dx.doi.org/10.5440/1430703, with a detailed description of model implementation, input files and various sensitivity analyses described in this paper.

20 Data sets used in this work can be found at https://dx.doi.org/10.5440/1168992 https://dx.doi.org/10.5440/1393836 https://dx.doi.org/10.5440/1288688 , and A synthesis of the incubation data is available at .

https://doi.org/10.5440/1440029 Author contributions

Competing interests

The authors declare no competing interests.

Acknowledgements

30

14

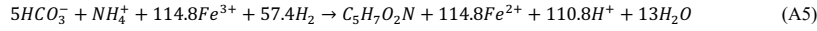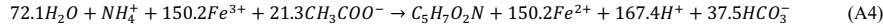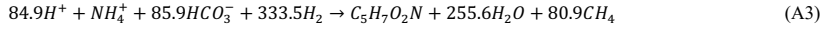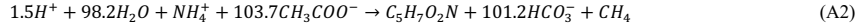**Appendix A: Anaerobic carbon decomposition model**

This section lists reactions used in the anaerobic carbon decomposition model. Under anaerobic conditions, dissolved organic carbon is converted to low molecular weight organic acids via fermentation. One simplified fermentation reaction is used to represent this lumped fermentation process, where 1/3 of the fermented organic carbon is converted to CO_2 (Tang et al., 2016; Xu et al., 2015):

$$C_6H_{12}O_6 + 4H_2O \rightarrow 2CH_3COO^- + 2HCO_3^- + 4H^+ + 4H_2 \tag{A1}$$
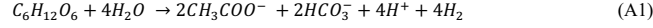
This fermentation reaction generates protons and decreases pH in the system. Fermentation products acetate and H_2 are further consumed via methanogenesis and iron reduction. The growth equations of methanogenesis and iron reduction were derived for each group using a thermodynamically-based approach, in which biomass synthesis is included in paired electron donor and electron acceptor half-reactions. A general molecular formula $C_5H_7O_2N$ is used for microbial biomass and the growth equations are written as (Istok et al., 2010)

$$1.5H^+ + 98.2H_2O + NH_4^+ + 103.7CH_3COO^- \rightarrow C_5H_7O_2N + 101.2HCO_3^- + CH_4 \tag{A2}$$

$$84.9H^+ + NH_4^+ + 85.9HCO_3^- + 333.5H_2 \rightarrow C_5H_7O_2N + 255.6H_2O + 80.9CH_4 \tag{A3}$$

$$72.1H_2O + NH_4^+ + 150.2Fe^{3+} + 21.3CH_3COO^- \rightarrow C_5H_7O_2N + 150.2Fe^{2+} + 167.4H^+ + 37.5HCO_3^- \tag{A4}$$

$$5HCO_3^- + NH_4^+ + 114.8Fe^{3+} + 57.4H_2 \rightarrow C_5H_7O_2N + 114.8Fe^{2+} + 110.8H^+ + 13H_2O \tag{A5}$$

In addition, Fe(III) concentration was calculated based on the dissolution of representative amorphous ferric hydroxides (A6), with a solubility constant $K_{s0} = 10^{3.96}$. This process consumes many protons and contributes to pH increases.

$$Fe(OH)_{3(s)} + 3H^+ \leftrightarrow Fe^{3+} + 3H_2O \tag{A6}$$

A complete set of rate constants used in this model can be found in Table S1.

Appendix B: Temperature and pH response functions

We used the CLM_CN temperature response function (B1) in our simulations (Thornton and Rosenbloom, 2005). Additional tested temperature response functions included B2 used by the CENTURY model (Parton et al., 2001), Arrhenius equation B3 used in *ecosys* (Grant, 1998), and the quadratic equation B4 (Ratkowsky et al., 1983). T_{ref} is set at 25 °C, E_a is the activation energy (J mol^{-1}), and R is the universal gas constant (J K^{-1} mol^{-1}). T_m used in Ratkowsky's model represents a conceptual temperature of no metabolic significance and is set at -8 °C in this study.

$$\ln f(T) = 308.56 \times \left(\frac{1}{71.02} - \frac{1}{T - 227.13}\right) \tag{B1}$$

$$f(T) = 0.56 + 0.465 \arctan\left[0.097(T - 15.7)\right] \tag{B2}$$

$$f(T) = e^{\frac{-E_a}{R}\left(\frac{1}{T} - \frac{1}{T_{ref}}\right)} \tag{B3}$$

$$f(T) = \left(\frac{T - T_m}{T_{ref} - T_m}\right)^2 \tag{B4}$$

The discontinuous bell-shaped pH response function from the DLEM model was used here (equation B5, Tian et al., 2010)

Deleted: which contributed

Deleted: increase

Deleted: ↔

Deleted: OH^-

Deleted: the

Deleted: significant

$$f(pH) = \frac{1.02}{1.02 + 10^6 \exp(-2.5pH)} \quad (0<pH<7) \hspace{2cm} (B5)$$

$$f(pH) = \frac{1.02}{1.02 + 10^6 \exp(-2.5(14-pH))} \quad (7<pH<14)$$

5

References

10   Atalay, Y. B., Carbonaro, R. F., and Di Toro, D. M.: Distribution of Proton Dissociation Constants for Model Humic and Fulvic Acid Molecules, Environmental Science & Technology, 43, 3626-3631, 10.1021/es803057r, 2009.

Bethke, C. M., Sanford, R. A., Kirk, M. F., Jin, Q., and Flynn, T. M.: The thermodynamic ladder in geomicrobiology, American Journal of Science, 311, 183-210, 10.2475/03.2011.01, 2011.

Blumer-Schuette, S. E., Brown, S. D., Sander, K. B., Bayer, E. A., Kataeva, I., Zurawski, J. V., Conway, J. M., Adams, M. W. W., and Kelly, R. M.: Thermophilic lignocellulose deconstruction, FEMS Microbiology Reviews, 38, 393-448, 10.1111/1574-6976.12044, 2014.

Bore, E. K., Apostel, C., Halicki, S., Kuzyakov, Y., and Dippold, M. A.: Microbial Metabolism in Soil at Subzero Temperatures: Adaptation Mechanisms Revealed by Position-Specific 13C Labeling, Frontiers in Microbiology, 8, 10.3389/fmicb.2017.00946, 2017.

20   Boye, K., Noël, V., Tfaily, M. M., Bone, S. E., Williams, K. H., Bargar, John R., and Fendorf, S.: Thermodynamically controlled preservation of organic carbon in floodplains, Nature Geoscience, 10, 415, 10.1038/ngeo2940, 2017.

Davidson, E. A., and Janssens, I. A.: Temperature sensitivity of soil carbon decomposition and feedbacks to climate change, Nature, 440, 165-173, 2006.

Drake, T. W., Wickland, K. P., Spencer, R. G. M., McKnight, D. M., and Striegl, R. G.: Ancient low–molecular-weight organic acids in permafrost fuel rapid carbon dioxide production upon thaw, Proceedings of the National Academy of Sciences, 112, 13946-13951, 10.1073/pnas.1511705112, 2015.

Ernakovich, J. G., Lynch, L. M., Brewer, P. E., Calderon, F. J., and Wallenstein, M. D.: Redox and temperature-sensitive changes in microbial communities and soil chemistry dictate greenhouse gas loss from thawed permafrost, Biogeochemistry, 134, 183-200, 10.1007/s10533-017-0354-5, 2017.

30   Glissmann, K., and Conrad, R.: Saccharolytic activity and its role as a limiting step in methane formation during the anaerobic degradation of rice straw in rice paddy soil, Biology and Fertility of Soils, 35, 62-67, 10.1007/s00374-002-0442-z, 2002.

Grant, R. F.: Simulation of methanogenesis in the mathematical model ecosys, Soil Biology and Biochemistry, 30, 883-896, http://dx.doi.org/10.1016/S0038-0717(97)00218-6, 1998.

35   Hansen, A. A., Herbert, R. A., Mikkelsen, K., Jensen, L. L., Kristoffersen, T., Tiedje, J. M., Lomstein, B. A., and Finster, K. W.: Viability, diversity and composition of the bacterial community in a high Arctic permafrost soil from Spitsbergen, Northern Norway, Environmental Microbiology, 9, 2870-2884, 10.1111/j.1462-2920.2007.01403.x, 2007.

Herndon, E. M., Yang, Z., Bargar, J., Janot, N., Regier, T. Z., Graham, D. E., Wullschleger, S. D., Gu, B., and Liang, L.: Geochemical drivers of organic matter decomposition in arctic tundra soils, Biogeochemistry, 126, 397-414, 40   10.1007/s10533-015-0165-5, 2015.

Høj, L., Rusten, M., Haugen, L. E., Olsen, R. A., and Torsvik, V. L.: Effects of water regime on archaeal community composition in Arctic soils, Environmental Microbiology, 8, 984-996, 10.1111/j.1462-2920.2006.00982.x, 2006.

Howell, J., Donahoe, R., Roden, E., and Ferris, F.: Effects of microbial iron oxide reduction on pH and alkalinity in anaerobic bicarbonate-buffered media: implications for metal mobility,

45   Istok, J. D., Park, M., Michalsen, M., Spain, A. M., Krumholz, L. R., Liu, C., McKinley, J., Long, P., Roden, E., Peacock, A. D., and Baldwin, B.: A thermodynamically-based model for predicting microbial growth and community composition coupled to system geochemistry: Application to uranium bioreduction, Journal of Contaminant Hydrology, 112, 1-14, https://doi.org/10.1016/j.jconhyd.2009.07.004, 2010.

Jin, Q., and Bethke, C. M.: A New Rate Law Describing Microbial Respiration, Applied and Environmental Microbiology, 69, 50   2340-2348, 10.1128/aem.69.4.2340-2348.2003, 2003.

Jin, Q., and Bethke, C. M.: The thermodynamics and kinetics of microbial metabolism, American Journal of Science, 307, 643-677, 10.2475/04.2007.01, 2007.

Jin, Q., and Kirk, M. F.: pH as a Primary Control in Environmental Microbiology: 1. Thermodynamic Perspective, Frontiers in Environmental Science, 6, 10.3389/fenvs.2018.00021, 2018.

55   Jones, D. L., Dennis, P. G., Owen, A. G., and van Hees, P. A. W.: Organic acid behavior in soils – misconceptions and knowledge gaps, Plant and Soil, 248, 31-41, 10.1023/a:1022304332313, 2003.

Karhu, K., Auffret, M. D., Dungait, J. A. J., Hopkins, D. W., Prosser, J. I., Singh, B. K., Subke, J.-A., Wookey, P. A., Agren, G. I., Sebastia, M.-T., Gouriveau, F., Bergkvist, G., Meir, P., Nottingham, A. T., Salinas, N., and Hartley, I. P.: Temperature sensitivity of soil respiration rates enhanced by microbial community response, Nature, 513, 81-84, 60   10.1038/nature13604, 2014.

Deleted: ¶

Knoblauch, C., Beer, C., Sosnin, A., Wagner, D., and Pfeiffer, E.-M.: Predicting long-term carbon mineralization and trace gas production from thawing permafrost of Northeast Siberia, Global Change Biology, 19, 1160-1172, 10.1111/gcb.12116, 2013.

Kotsyurbenko, O. R.: Trophic interactions in the methanogenic microbial community of low-temperature terrestrial ecosystems, FEMS Microbiology Ecology, 53, 3-13, http://dx.doi.org/10.1016/j.femsec.2004.12.009, 2005.

Koven, C. D., Riley, W. J., Subin, Z. M., Tang, J. Y., Torn, M. S., Collins, W. D., Bonan, G. B., Lawrence, D. M., and Swenson, S. C.: The effect of vertically resolved soil biogeochemistry and alternate soil C and N models on C dynamics of CLM4, Biogeosciences, 10, 7109-7131, 10.5194/bg-10-7109-2013, 2013.

Koven, C. D., Lawrence, D. M., and Riley, W. J.: Permafrost carbon−climate feedback is sensitive to deep soil carbon decomposability but not deep soil nitrogen dynamics, Proceedings of the National Academy of Sciences, 112, 3752-3757, 10.1073/pnas.1415123112, 2015.

Lawrence, D. M., Koven, C. D., Swenson, S. C., Riley, W. J., and Slater, A. G.: Permafrost thaw and resulting soil moisture changes regulate projected high-latitude CO_2 and CH_4 emissions, Environmental Research Letters, 10, 094011, 2015.

Lee, H., Schuur, E. A. G., Inglett, K. S., Lavoie, M., and Chanton, J. P.: The rate of permafrost carbon release under aerobic and anaerobic conditions and its potential effects on climate, Global Change Biology, 18, 515-527, 10.1111/j.1365-2486.2011.02519.x, 2012.

Lipson, D. A., Jha, M., Raab, T. K., and Oechel, W. C.: Reduction of iron (III) and humic substances plays a major role in anaerobic respiration in an Arctic peat soil, Journal of Geophysical Research: Biogeosciences, 115, n/a-n/a, 10.1029/2009JG001147, 2010.

Lipson, D. A., Raab, T. K., Goria, D., and Zlamal, J.: The contribution of Fe(III) and humic acid reduction to ecosystem respiration in drained thaw lake basins of the Arctic Coastal Plain, Global Biogeochemical Cycles, 27, 399-409, 10.1002/gbc.20038, 2013.

Lupascu, M., Wadham, J. L., Hornibrook, E. R. C., and Pancost, R. D.: Temperature Sensitivity of Methane Production in the Permafrost Active Layer at Stordalen, Sweden: A Comparison with Non-permafrost Northern Wetlands, Arctic, Antarctic, and Alpine Research, 44, 469-482, 10.1657/1938-4246-44.4.469, 2012.

MacDougall, A. H., Avis, C. A., and Weaver, A. J.: Significant contribution to climate warming from the permafrost carbon feedback, Nature Geosci, 5, 719-721, http://www.nature.com/ngeo/journal/v5/n10/abs/ngeo1573.html#supplementary-information, 2012.

McGuire, A. D., Christensen, T. R., Hayes, D., Heroult, A., Euskirchen, E., Kimball, J. S., Koven, C., Lafleur, P., Miller, P. A., Oechel, W., Peylin, P., Williams, M., and Yi, Y.: An assessment of the carbon balance of Arctic tundra: comparisons among observations, process models, and atmospheric inversions, Biogeosciences, 9, 3185-3204, 10.5194/bg-9-3185-2012, 2012.

Meng, L., Hess, P. G. M., Mahowald, N. M., Yavitt, J. B., Riley, W. J., Subin, Z. M., Lawrence, D. M., Swenson, S. C., Jauhiainen, J., and Fuka, D. R.: Sensitivity of wetland methane emissions to model assumptions: application and model testing against site observations, Biogeosciences, 9, 2793-2819, 10.5194/bg-9-2793-2012, 2012.

Newman, B. D., Throckmorton, H. M., Graham, D. E., Gu, B., Hubbard, S. S., Liang, L., Wu, Y., Heikoop, J. M., Herndon, E. M., Phelps, T. J., Wilson, C. J., and Wullschleger, S. D.: Microtopographic and depth controls on active layer chemistry in Arctic polygonal ground, Geophysical Research Letters, 42, 1808-1817, 10.1002/2014GL062804, 2015.

Ratkowsky, D. A., Olley, J., McMeekin, T. A., and Ball, A.: Relationship between temperature and growth rate of bacterial cultures, Journal of Bacteriology, 149, 1-5, 1982.

Ratkowsky, D. A., Lowry, R. K., McMeekin, T. A., Stokes, A. N., and Chandler, R. E.: Model for bacterial culture growth rate throughout the entire biokinetic temperature range, Journal of Bacteriology, 154, 1222-1226, 1983.

Riley, W. J., Subin, Z. M., Lawrence, D. M., Swenson, S. C., Torn, M. S., Meng, L., Mahowald, N. M., and Hess, P.: Barriers to predicting changes in global terrestrial methane fluxes: analyses using CLM4Me, a methane biogeochemistry model integrated in CESM, Biogeosciences, 8, 1925-1953, 10.5194/bg-8-1925-2011, 2011.

Rivkina, E., Shcherbakova, V., Laurinavichius, K., Petrovskaya, L., Krivushin, K., Kraev, G., Pecheritsina, S., and Gilichinsky, D.: Biogeochemistry of methane and methanogenic archaea in permafrost, FEMS Microbiology Ecology, 61, 1-15, 10.1111/j.1574-6941.2007.00315.x, 2007.

Roy Chowdhury, T., Herndon, E. M., Phelps, T. J., Elias, D. A., Gu, B., Liang, L., Wullschleger, S. D., and Graham, D. E.: Stoichiometry and temperature sensitivity of methanogenesis and CO2 production from saturated polygonal tundra in Barrow, Alaska, Global Change Biology, 21, 722-737, 10.1111/gcb.12762, 2015.

Schädel, C., Luo, Y., David Evans, R., Fei, S., and Schaeffer, S. M.: Separating soil CO2 efflux into C-pool-specific decay rates via inverse analysis of soil incubation data, Oecologia, 171, 721-732, 10.1007/s00442-012-2577-4, 2013.

Schädel, C., Schuur, E. A. G., Bracho, R., Elberling, B., Knoblauch, C., Lee, H., Luo, Y., Shaver, G. R., and Turetsky, M. R.: Circumpolar assessment of permafrost C quality and its vulnerability over time using long-term incubation data, Global Change Biology, 20, 641-652, 10.1111/gcb.12417, 2014.

Schaefer, K., Hugues, L., Vladimir, E. R., Edward, A. G. S., and Ronald, W.: The impact of the permafrost carbon feedback on global climate, Environmental Research Letters, 9, 085003, 2014.

Schuur, E. A. G., Vogel, J. G., Crummer, K. G., Lee, H., Sickman, J. O., and Osterkamp, T. E.: The effect of permafrost thaw on old carbon release and net carbon exchange from tundra, Nature, 459, 556-559, http://www.nature.com/nature/journal/v459/n7246/suppinfo/nature08031_S1.html, 2009.

Schuur, E. A. G., McGuire, A. D., Schadel, C., Grosse, G., Harden, J. W., Hayes, D. J., Hugelius, G., Koven, C. D., Kuhry, P., Lawrence, D. M., Natali, S. M., Olefeldt, D., Romanovsky, V. E., Schaefer, K., Turetsky, M. R., Treat, C. C., and Vonk, J. E.: Climate change and the permafrost carbon feedback, Nature, 520, 171-179, 10.1038/nature14338, 2015.

5 Segers, R.: Methane production and methane consumption: a review of processes underlying wetland methane fluxes, Biogeochemistry, 41, 23-51, 10.1023/a:1005929032764, 1998.

Tang, G., Zheng, J., Xu, X., Yang, Z., Graham, D. E., Gu, B., Painter, S. L., and Thornton, P. E.: Biogeochemical modeling of CO_2 and CH_4 production in anoxic Arctic soil microcosms, Biogeosciences, 13, 5021-5041, 10.5194/bg-13-5021-2016, 2016.

Tarnocai, C., Canadell, J. G., Schuur, E. A. G., Kuhry, P., Mazhitova, G., and Zimov, S.: Soil organic carbon pools in the northern circumpolar permafrost region, Global Biogeochemical Cycles, 23, GB2023, 10.1029/2008GB003327, 2009.

10 Thornton, P. E., and Rosenbloom, N. A.: Ecosystem model spin-up: Estimating steady state conditions in a coupled terrestrial carbon and nitrogen cycle model, Ecological Modelling, 189, 25-48, https://doi.org/10.1016/j.ecolmodel.2005.04.008, 2005.

Tian, H., Xu, X., Liu, M., Ren, W., Zhang, C., Chen, G., and Lu, C.: Spatial and temporal patterns of CH_4 and N_2O fluxes in terrestrial ecosystems of North America during 1979–2008: application of a global biogeochemistry model, Biogeosciences, 7, 2673-2694, 10.5194/bg-7-2673-2010, 2010.

15 Tilston, E. L., Sparrman, T., and Öquist, M. G.: Unfrozen water content moderates temperature dependence of sub-zero microbial respiration, Soil Biology and Biochemistry, 42, 1396-1407, https://doi.org/10.1016/j.soilbio.2010.04.018, 2010.

Treat, C. C., Wollheim, W. M., Varner, R. K., Grandy, A. S., Talbot, J., and Frolking, S.: Temperature and peat type control CO2 and CH4 production in Alaskan permafrost peats, Global Change Biology, 20, 2674-2686, 10.1111/gcb.12572, 2014.

Treat, C. C., Natali, S. M., Ernakovich, J., Iversen, C. M., Lupascu, M., McGuire, A. D., Norby, R. J., Roy Chowdhury, T.,
20 Richter, A., Šantrůčková, H., Schädel, C., Schuur, E. A. G., Sloan, V. L., Turetsky, M. R., and Waldrop, M. P.: A pan-Arctic synthesis of CH4 and CO2 production from anoxic soil incubations, Global Change Biology, 21, 2787-2803, 10.1111/gcb.12875, 2015.

Tuomi, M., Vanhala, P., Karhu, K., Fritze, H., and Liski, J.: Heterotrophic soil respiration—Comparison of different models describing its temperature dependence, Ecological Modelling, 211, 182-190,
25 https://doi.org/10.1016/j.ecolmodel.2007.09.003, 2008.

Vaughn, L. J. S., Conrad, M. E., Bill, M., and Torn, M. S.: Isotopic insights into methane production, oxidation, and emissions in Arctic polygon tundra, Global Change Biology, 22, 3487-3502, 10.1111/gcb.13281, 2016.

Wachinger, G., Fiedler, S., Zepp, K., Gattinger, A., Sommer, M., and Roth, K.: Variability of soil methane production on the micro-scale: spatial association with hot spots of organic material and Archaeal populations, Soil Biology and
30 Biochemistry, 32, 1121-1130, https://doi.org/10.1016/S0038-0717(00)00024-9, 2000.

Wagner, R., Zona, D., Oechel, W., and Lipson, D.: Microbial community structure and soil pH correspond to methane production in Arctic Alaska soils, Environmental Microbiology, 19, 3398-3410, 10.1111/1462-2920.13854, 2017.

Waldrop, M. P., Wickland, K. P., White Iii, R., Berhe, A. A., Harden, J. W., and Romanovsky, V. E.: Molecular investigations into a globally important carbon pool: permafrost-protected carbon in Alaskan soils, Global Change Biology, 16, 2543-
35 2554, 10.1111/j.1365-2486.2009.02141.x, 2010.

Xu, X., Elias, D. A., Graham, D. E., Phelps, T. J., Carroll, S. L., Wullschleger, S. D., and Thornton, P. E.: A microbial functional group-based module for simulating methane production and consumption: Application to an incubated permafrost soil, Journal of Geophysical Research: Biogeosciences, 120, 1315-1333, 10.1002/2015JG002935, 2015.

Xu, X., Yuan, F., Hanson, P. J., Wullschleger, S. D., Thornton, P. E., Riley, W. J., Song, X., Graham, D. E., Song, C., and Tian,
40 H.: Reviews and syntheses: Four decades of modeling methane cycling in terrestrial ecosystems, Biogeosciences, 13, 3735-3755, 10.5194/bg-13-3735-2016, 2016.

Yang, S., Liebner, S., Winkel, M., Alawi, M., Horn, F., Dörfer, C., Ollivier, J., He, J.-s., Jin, H., Kühn, P., Schloter, M., Scholten, T., and Wagner, D.: In-depth analysis of core methanogenic communities from high elevation permafrost-affected wetlands, Soil Biology and Biochemistry, 111, 66-77, https://doi.org/10.1016/j.soilbio.2017.03.007, 2017.

45 Yang, Z., Wullschleger, S. D., Liang, L., Graham, D. E., and Gu, B.: Effects of warming on the degradation and production of low-molecular-weight labile organic carbon in an Arctic tundra soil, Soil Biology and Biochemistry, 95, 202-211, http://dx.doi.org/10.1016/j.soilbio.2015.12.022, 2016.

Yvon-Durocher, G., Caffrey, J. M., Cescatti, A., Dossena, M., Giorgio, P. d., Gasol, J. M., Montoya, J. M., Pumpanen, J., Staehr, P. A., Trimmer, M., Woodward, G., and Allen, A. P.: Reconciling the temperature dependence of respiration across
50 timescales and ecosystem types, Nature, 487, 472-476, 2012.

Yvon-Durocher, G., Allen, A. P., Bastviken, D., Conrad, R., Gudasz, C., St-Pierre, A., Thanh-Duc, N., and del Giorgio, P. A.: Methane fluxes show consistent temperature dependence across microbial to ecosystem scales, Nature, 507, 488-491, 10.1038/nature13164, 2014.

Zhalnina, K., Dias, R., de Quadros, P. D., Davis-Richardson, A., Camargo, F. A., Clark, I. M., McGrath, S. P., Hirsch, P. R., and
55 Triplett, E. W.: Soil pH determines microbial diversity and composition in the park grass experiment, Microbial ecology, 69, 395-406, 10.1007/s00248-014-0530-2, 2015.

Zheng, J., and Graham, D.: Soil Organic Carbon Degradation in Low Temperature Soil Incubations from Flat- and High-Centered Polygons, Barrow, Alaska, 2012-2013. Next Generation Ecosystem Experiments Arctic Data Collection, Oak Ridge National Laboratory, U.S. Department of Energy, Oak Ridge, Tennessee, USA. Dataset accessed on [date] at
60 http://dx.doi.org/10.5440/1393836., 2017.

Zhuang, Q., Melillo, J. M., Sarofim, M. C., Kicklighter, D. W., McGuire, A. D., Felzer, B. S., Sokolov, A., Prinn, R. G., Steudler, P. A., and Hu, S.: CO2 and CH4 exchanges between land ecosystems and the atmosphere in northern high latitudes over the 21st century, Geophysical Research Letters, 33, n/a-n/a, 10.1029/2006GL026972, 2006.

Zimov, S. A., Schuur, E. A. G., and Chapin, F. S.: Permafrost and the Global Carbon Budget, Science, 312, 1612-1613, 10.1126/science.1128908, 2006.

5

10

19
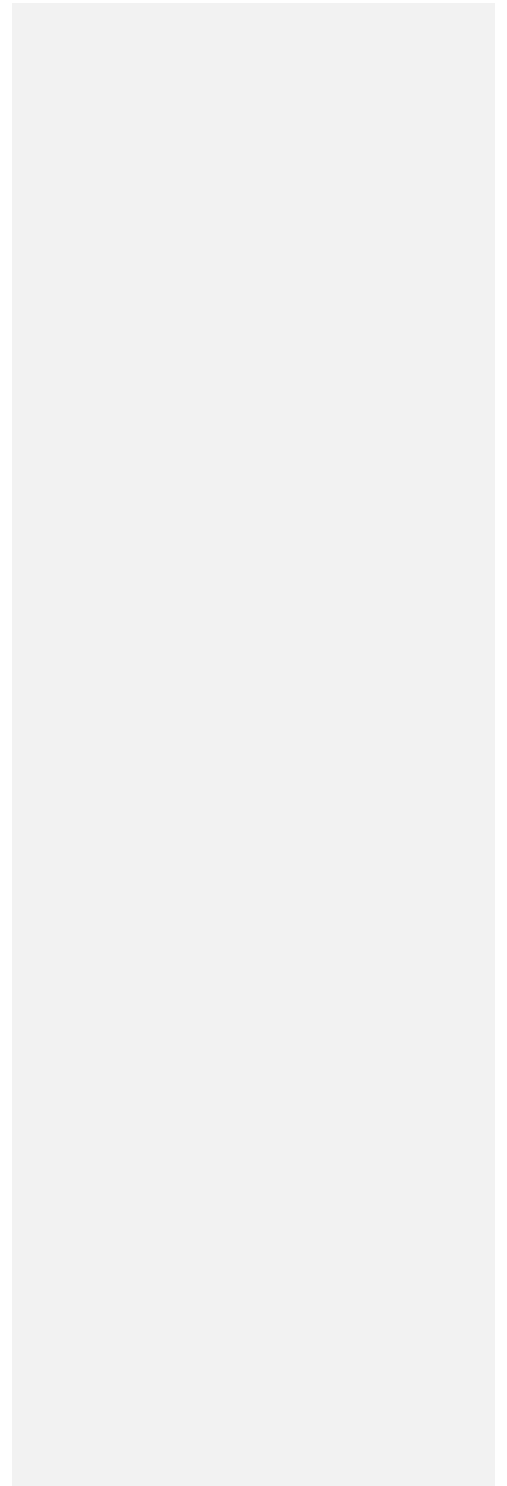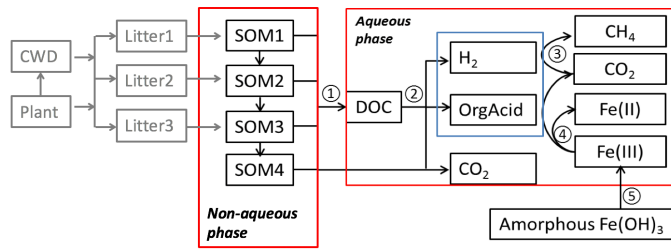
Figure 1. Conceptual diagram showing key processes in the anaerobic carbon decomposition framework. The numbers indicate different processes: 1. SOM degradation from soil organic carbon pools with increasing turnover time produces dissolved organic carbon (DOC) and CO_2; 2. Fermentation of DOC into organic acids, H_2 and CO_2; 3. Methanogenesis from organic acids or H_2; 4. Fe(III) reduction from organic acids or H_2. 5. Fe(OH)$_3$ dissolution.

Deleted: Empirical

5
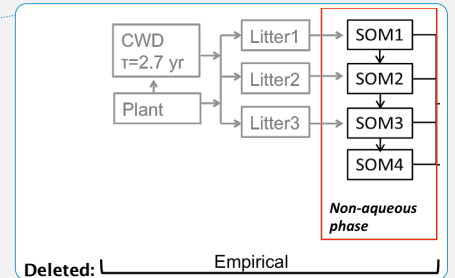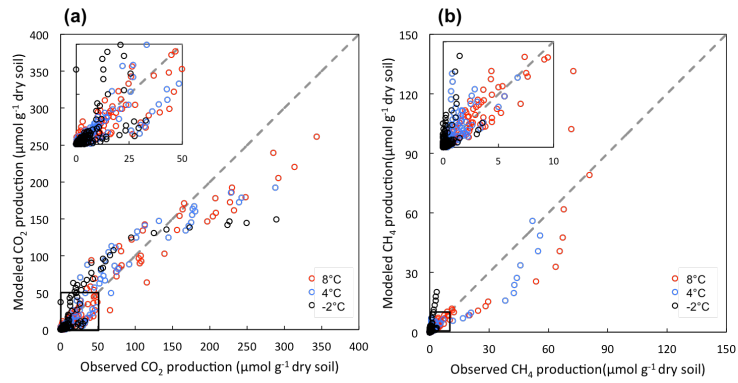
Figure 2. Comparison between modeled and observed production of CO_2 (a) and CH_4 (b). Averaged measurements of
10 **triplicate microcosms at each time point from each incubation temperature were calculated as observed values.**

21
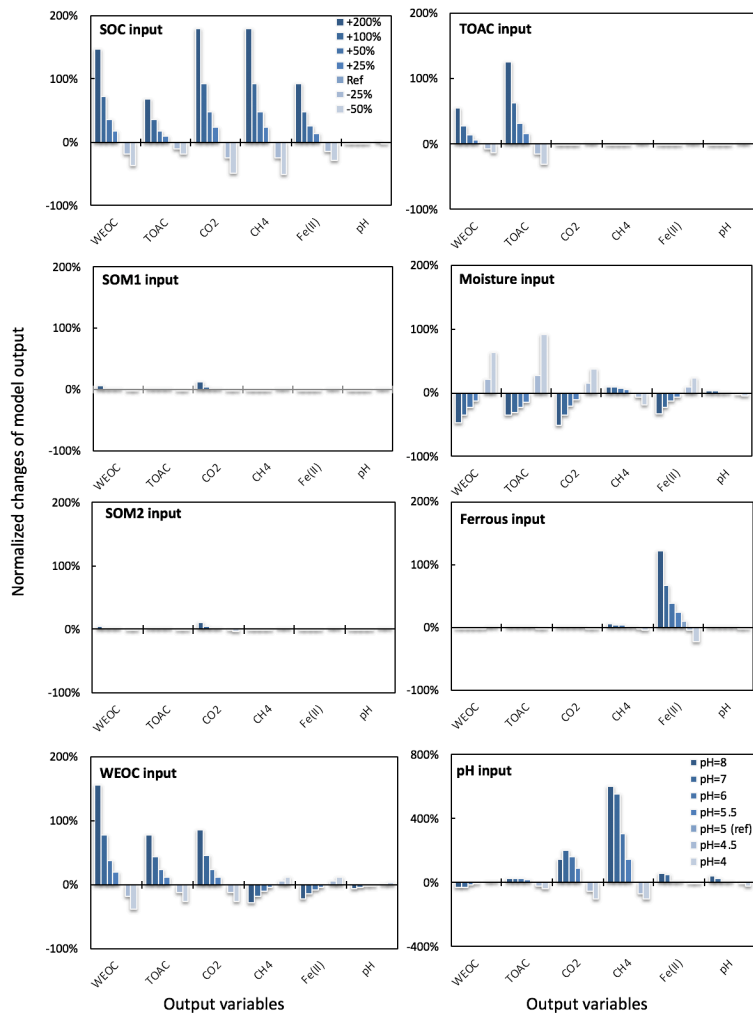
Figure 3. Perturbations of initial soil geochemical conditions differentially affected model predictions (including CH_4, CO_2, Fe(II), TOAC, WEOC, and pH) during anaerobic carbon decomposition. For example, when the initial pH decreased by 8% and 17%, CH4 production decreased by 40% and 80%, respectively. Normalized changes in model output were calculated as the ratio of changes caused by perturbation simulations (differences between perturbation and reference runs) to reference simulation output after 60 days of anaerobic decomposition at 8 °C. To test model sensitivity in response to initial pH, the reference run started with pH 6, and up to 1 pH unit changes was applied in perturbation simulations to represent a realistic pH range for soils. Reference simulations were based on soils with 30% SOC (water content=2 g g^{-1} dwt, and pH=5).
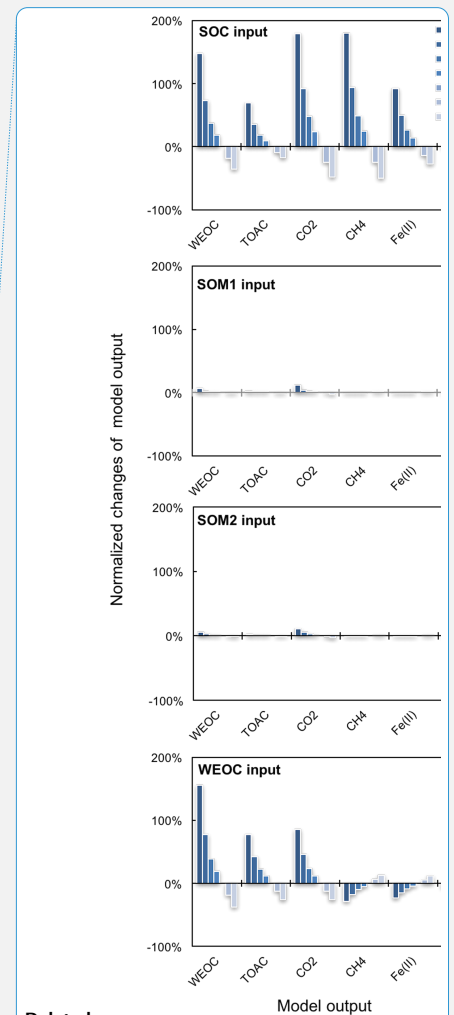
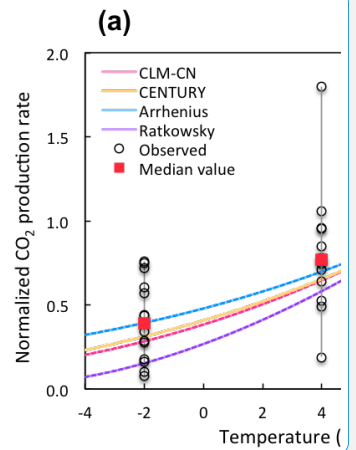Deleted:

Deleted: simulation output

22

5
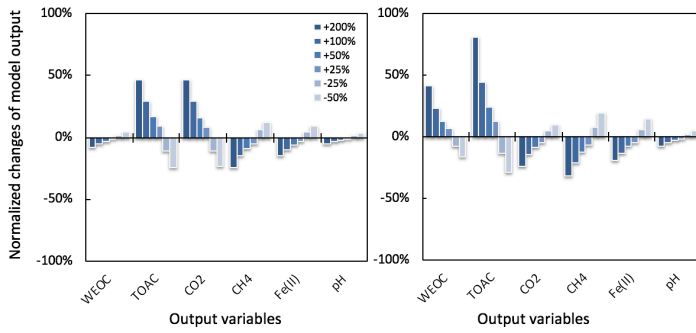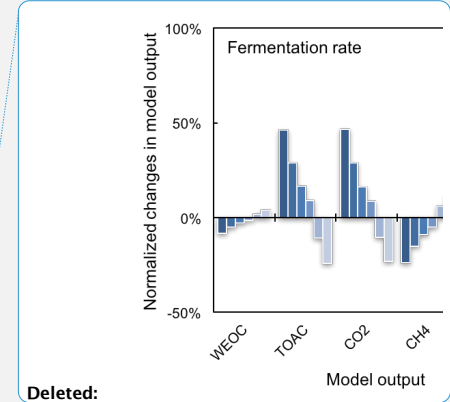
Figure 4. Simulated changes in model predictions (including CH₄, CO₂, Fe(II), TOAC, WEOC, and pH) during anaerobic carbon decomposition in response to perturbations of (a) fermentation rate and (b) fermentation stoichiometry (Acetate:CO₂=1:1 for reference simulation). Normalized changes in model output were calculated as the ratio of perturbation simulation output to reference simulation output after 60 days of anaerobic decomposition at 8 °C. Reference simulations were based on soils with 30% SOC (water content=2 g g⁻¹ dwt, and pH=5).

(a)

(b)
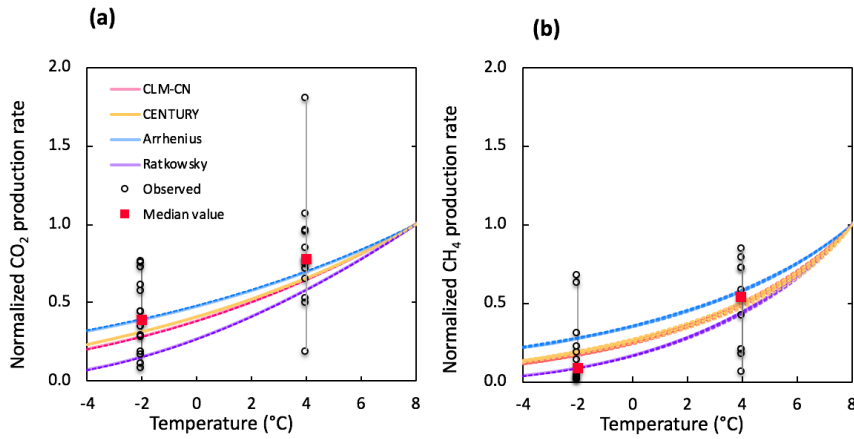
Figure 5. Comparison of simulated and observed temperature response for the production of CO_2 (a) and CH_4 (b). Results were all normalized to CO_2 or CH_4 production rates at 8 °C for direct comparison. Observations at -2 °C and 4 °C were plotted in black dots and the median value were marked in red. The shaded area represents output uncertainties generated from rate estimations within 60 ± 5 days. Reference simulations were based on soils with 30% SOC (water content=2 g g^{-1} dwt, and pH=5).
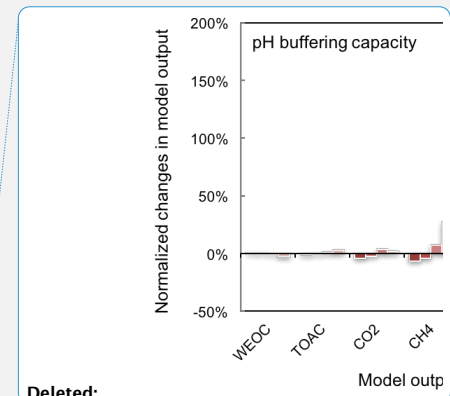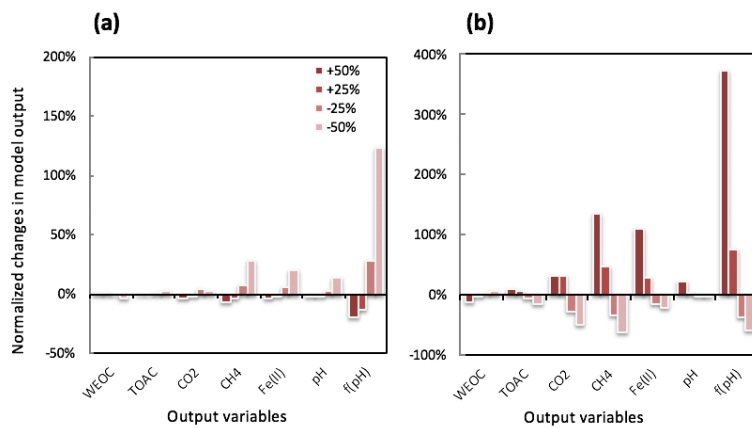
Deleted:

Deleted: ±

Figure 6. Simulated changes in model predictions (including CH$_4$, CO$_2$, Fe(II), TOAC, WEOC, pH and f_{pH}) during anaerobic carbon decomposition in response to perturbations of (a) pH buffering capacity, and (b) pH response function. Normalized changes in model output were calculated as the ratio of perturbation simulation output to reference simulation output after 60 days of anaerobic decomposition at 8 °C. Reference simulations were based on soils with 30% SOC (water content=2 g g^{-1} dwt, and pH=5).
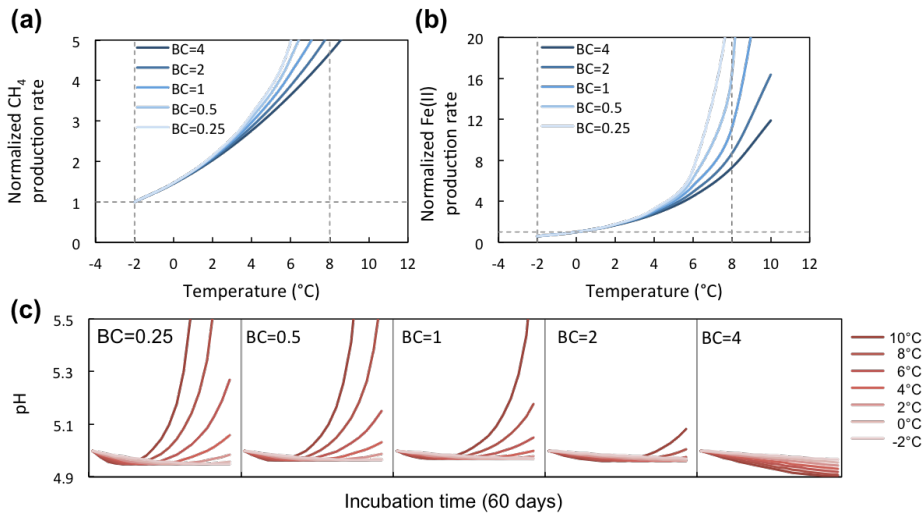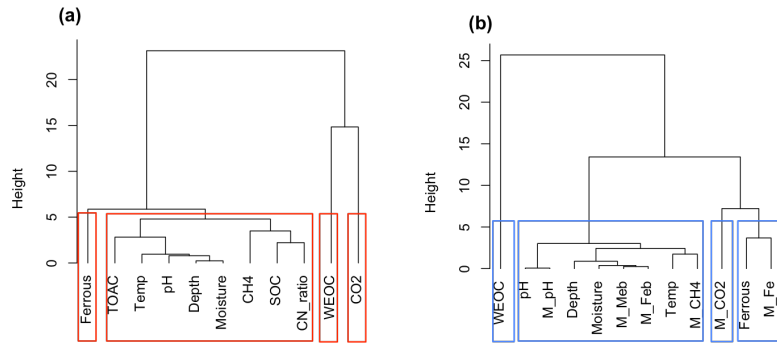
Figure 7. Temperature response of CH₄ and Fe(II) production rates at varying soil pH buffering capacities (BC). Varying BCs with respect to the reference simulation (BC=1) creates strong feedback to rates of methanogenesis and iron reduction. Reference simulations were based on soils with 30% SOC (water content=2 g g⁻¹ dwt, and pH=5).

Figure 8. Cluster analysis of soil geochemical properties related to CO_2 and CH_4 production using Ward's linkage method. (a) cluster analysis of measured soil geochemical characteristics and observed CO_2 and CH_4 production (*n*=42); (b) cluster analysis of modeled results (*n*=42). Model simulated CO_2, CH_4, and Fe(II) production and final pH are labeled as M_CO2, M_CH4, M_Fe, and M_pH, respectively. Biomasses of methanogens and iron reducers were tracked in the model and labeled M_Meb and M_Feb, respectively.

| Deleted: Biomass |
| Deleted: as |
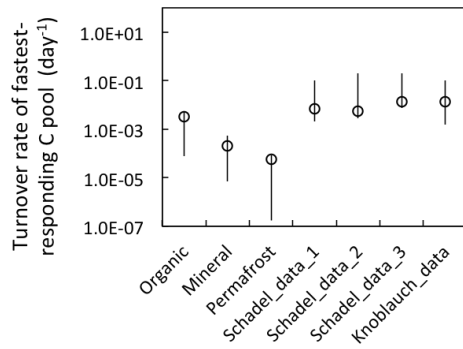
Figure 9. Model estimated turnover rates of the fastest-decomposing carbon pool. Organic, Mineral, and Permafrost labels represent estimations from our model simulations (rates estimated at 4 °C). Schadel_data represent turnover rates estimated via a three-pool model from pooled anaerobic incubations with normalized incubation temperature of 5 °C (tag 1, 2, and 3 represent pool estimation from different soil types: 1. Organic, 2, Mineral <1m, 3. Mineral >1m) . Knoblauch_data are rate estimates (at 4 °C) made via a two-pool model (Schädel et al., 2014;Knoblauch et al., 2013). Open symbols represent the average values, and the vertical lines represent the estimated range.